MIXED CONVECTION IN A DRIVEN CAVITY WITH AN INTERNAL OBSTACLE USING THE LATTICE BOLTZMANN METHOD

by

Muhammad Ayaz HAFEEZ [*] ***and Shams ul ISLAM***

Department of Mathematics, COMSATS University Islamabad, Islamabad Campus, Pakistan

Original scientific paper
https://doi.org/10.2298/TSCI220216109H

The flow and heat transport of a viscous fluid contained in a square cavity have been extensively studied using parametric analysis. Lattice Boltzmann method is used to simulate fluid-flow in a square lid-driven cavity with a square-shaped obstacle in the cavity's centre. The cavity's top wall generates flow that moves at a constant speed in its own plane and is maintained at a higher temperature than the bottom wall. Reynolds number, Rayleigh number, Prandtl number, Grashof number, and Richardson number are the primary parameters used in this study. The relevance of natural and forced convection, contributions of conduction, and convection to total heat transfer are estimated. The influence of the temperature of the obstacle on the velocity and temperature of the fluid is also being investigated. When, Ri ≪ 1, the temperature of the obstacle has almost negligible influence on fluid velocity, the fluids are well mixed, and temperature fluctuations are minor in the bulk of the cavity interior. When, Ri ≫ 1, the obstacle's temperature, has a considerable impact on fluid velocity, much of the fluid in the cavity's middle and bottom regions remains stationary. These regions have a vertically linear temperature distribution. Further studies were carried out to investigate how the Prandtl number influenced the fluid's temperature. The findings are presented as contour plots of velocity and temperature, streamlines, horizontal and vertical velocity profiles, and vertical temperature profiles.

Key words: *mixed convection, lid-driven, square cavity, lattice Boltzmann method*

Introduction

One of the most basic restricted geometries in which fluid motion may be investigated is the rectangle, or cubic container. The tangential in-plane movement of the bounding wall is the most important mechanical driving force that acts on a flowing liquid with constant density while maintaining a simple domain. A cuboid with one of its bounding walls moving tangentially to itself is known as a lid-driven cavity. Because of its simplicity, the lid-driven cavity has received a lot of attention. It is been used as both a numerical benchmark problem and a test bed for investigating specific physical phenomena. The Reynolds number and the cavity aspect ratio, which are defined as $\mathrm{Re} = U_o h/\nu$ and $A = h/b$, respectively, are the two most important non-dimensional variables that characterize the flow. Here h and b are the

[*]Corresponding author, e-mail: muhammadayazhafeez@gmail.com

height and breadth of the cavity, ν is the fluid's kinematic viscosity, and U_o is the speed of top bounding wall. The results of numerical computational investigations have been previously investigated in the literature [1-9] as well as the concordance between these computational estimates and actual experiments [2, 4].

When a temperature gradient is introduced into the cavity side walls, it provides a major dynamical factor. The temperature difference generates a buoyancy effect, which affects the cavity's velocity and temperature. Understanding this mixed-driven natural convective flow with internal impediments contributes to a better understanding of fundamental fluid dynamics and real-world engineering problems. A review of the literature revealed that investigations into mixed convection inside a closed cavity with obstacles are fairly frequent. The findings of numerical investigations of mixed convective flow in a hollow square cavity were published by Iwastu *et al.* [10]. They expanded on Mohamad and Viskanta's [11] work in their research. Mohammad and Viskanta [11] published the findings of numerical studies of mixed convective flow in a shallow cavity with $A \ll 1$. It is worth mentioning that in their study, the temperature of the main sliding wall was lower than the temperature of the fixed bottom wall. Thermal insulation was applied to the two vertical side walls. As a result, the flow became gravitationally unstable.

Iwastu *et al.* [10] examined the problem by maintaining a higher temperature on the upper sliding wall than on the bottom wall. They investigated a system that was gravitationally stable and had fluid-flow because of a top sliding wall. In such a case, only conduction was responsible for heat transport. As aforementioned, the majority of heat transport occurred by conduction, which was aided by forced convection. They also imposed a constant vertical temperature differential throughout the system. The key objective of their research was to properly explain the increase in heat transfer rate and provide velocity fields that were produced by moving the top wall in its own plane at a constant velocity using an external force. To cover the larger spectrum of flow characteristics, they employed a wide range of Reynolds and Rayleigh numbers.

In the last two decades, mixed convection had been studied using lattice Boltzmann method (LBM) in a driven cavity with various types of fluids and boundary conditions [12-16]. Karimipour *et al.* [12] used a Cu-water nanofluid to study mixed convection in an inclined cavity. They investigated mixed convection and discovered that for Ri = 0.1, Ri = 1, and Ri = 10, forced convection, mixed convection, and natural convection dominate, respectively. Guo *et al.* [13] investigated mixed convection for a variety of aspect ratios and Richardson number. They discovered that the Richardson number can be used to determine the relative significance of natural and forced convection modes in heat transport. Bettaibi *et al.* [14] used multiple relaxation times LBM to investigate mixed convection in a differentially heated cavity and discovered that heat transmitted in terms of Nusselt number rose as Richardson number decreased. Abu-Nada *et al.* [15] investigated mixed convection by flowing a nanofluid through a square chamber with a wavy bottom wall. They discovered that the introduction of nanoparticles increased heat transmission significantly for all values of the Richardson number. Using a wide range of Hartmann numbers, Oztop *et al.* [16] they investigated mixed convection in a driven cavity in the presence of a magnetic field with a heated bottom corner. They discovered that raising the Hartmann number reduces heat transmission. As a result, the magnetic field is vital in controlling heat transmission and fluid movement.

Ouhroum *et al.* [17] recently investigated mixed convection in a cavity with various baffle sizes and positions. In the present account, we investigate the same problem with a square-shaped solid obstacle placed in the cavity's centre. To complete this work, three sepa-

rate cases are studied. In Case 1, the flow behaviour is investigated in a simple cavity, like in Iwastu's *et al.* [10] paper. In Case 2, an obstacle is put in the centre of the cavity and kept at zero temperature. In Case 3, the obstacle is kept at the same high temperature as the top sliding wall.

Because we are investing flow in a square cavity, the length to width ratio, commonly known as the aspect ratio, is 1. Prandtl number is set to 0.71 in most cases because this permits the computation of the explicit impacts of forced convection, represented by Reynolds number and natural convection, represented by Grashof number.

Mixed convection is among some of the hot topics in thermodynamics because of its uses in many important industrial applications, such as in the cooling of electronic equipment, nuclear reactors, microelectronic devices, float glass manufacturing, electrical components, *etc*. The fundamental purpose of this research is to demonstrate a significant increase in global heat transmission and the influence of heated and cold obstacles on temperature distribution above that provided by the conductive mode, as well as the effects of obstacles on the velocity of the fluid in the cavity. The sliding top surface wall creates forced convection, which accomplishes this. This study also focuses on the influence of hot and cold impediments on the temperature and flow of fluid within the cavity. The cavity's upper wall is moving at a consistent velocity U_o while bottom wall is at rest. At the cavity's walls, bounce back boundary conditions with known velocity are imposed.

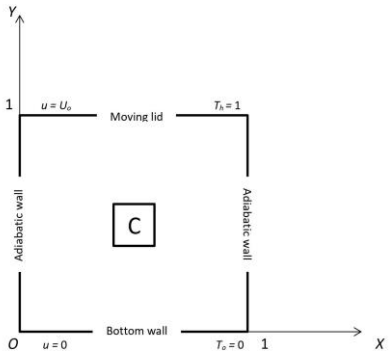

Figure 1. Flow configuration

Statement of the problem

The schematic flow of the problem is represented in fig. 1. A Cartesian co-ordinate system is used to represent the computing domain, with the origin in the cavity's bottom left corner. A square cavity with one unit of length on each side and a solid square shaped body, *C*, is placed in the cavity's centre build up the whole system. The bounce-back boundary conditions are simple and straight conditions that are used to describe solid, static, or dynamic boundary conditions. Because the top wall moves at a consistent speed, bounce-back boundary conditions with a known velocity are implemented on the top wall. At the obstacle's boundary, bounce back boundary conditions are implemented. The side walls of the cavity are considered adiabatic, whereas the upper wall is at temperature, T_h, and the bottom wall is at a lower temperature, T_o. According to the problem statement, the boundary conditions are:

$$\text{At} \quad y = 1, \quad 0 \leqslant x \leqslant 1, \quad \boldsymbol{u} = (U_o, 0) \quad \text{and} \quad T = T_h = 1$$

$$\text{At} \quad x = 0, \quad \text{and} \quad 1, \quad 0 \leqslant y \leqslant 1, \quad \boldsymbol{u} = 0 \quad \text{and} \quad \frac{\partial T}{\partial x} = 0$$

$$\text{At} \quad y = 0, \quad 0 \leqslant x \leqslant 1, \quad \boldsymbol{u} = 0 \quad \text{and} \quad T = T_o = 0$$

Methodology

The Navier-Stokes (NS) equations serve as the basis for CFD. The macroscopic characteristics of a fluid, such as temperature, velocity, and pressure, are commonly computed

using finite volume, finite difference, and finite element methodologies. These approaches transform governing differential equations with specific boundary and initial conditions to a system of algebraic equation. For incompressible fluid-flow, the governing equations for our problem are presented in non-dimensionalized form are continuity equation:

$$\nabla \boldsymbol{u} = 0 \tag{1}$$

momentum equation

$$\partial_t \boldsymbol{u} + (\boldsymbol{u}\nabla)\boldsymbol{u} = -\nabla p + \mathrm{Re}^{-1}\nabla^2 \boldsymbol{u} + \frac{\mathrm{Gr}}{\mathrm{Re}^2} T\boldsymbol{e} \tag{2}$$

and energy equation

$$\partial_t T + (\boldsymbol{u}\nabla)T = \frac{1}{\mathrm{PrRe}}\nabla^2 T \tag{3}$$

using the usual Boussinesq approximation [18]. It is a method for solving non-isothermal flow without solving the compressible NS equations. Variations in density are assumed to have no effect on the flow field other than to cause buoyancy forces. The macroscopic velocities are represented by $\boldsymbol{u} = (u,v)$. The density of the fluid, pressure field, temperature, and kinematic viscosity are represented by ρ, p, T, and ν, respectively, ∇ is the nabla operator and $\boldsymbol{e} = (0,1)$ represents a unit vector heading in the direction of buoyancy force.

The NS equations can be solved indirectly using LBM. The LBM is a comparatively modern way to understand the essence of fluids, and it is a solid method in the field of CFD, with a significant advantage over traditional computational approaches. It has a very vast range of applications in the modelling of incompressible flows in image processing, biomedical flows, blood vessel flows, multiphase flows, porous medium flows, chemical reactions, and other fields.

A distribution function represents the property of a collection of fluid particles. For the flow and temperature fields, the double population thermal LBM employs two separate distribution functions, F and G, respectively, for incompressible thermal flow problems [19, 20]. After applying the Bhatnagar-Gross-Krook (BGK) approximation [21], the discretized form of the governing equation of LBM-BGK [22] can be written.

In order to compute flow:

$$F_i(\boldsymbol{r} + \xi_i \Delta t, t + \Delta t) - F_i(\boldsymbol{r}, t) = -\frac{\Delta t}{\tau_v}\left[F_i(\boldsymbol{r}, t) - F_i^{\mathrm{eq}}(\boldsymbol{r}, t)\right] + f \tag{4}$$

In order to compute temperature:

$$G_i(\boldsymbol{r} + \xi_i \Delta t, t + \Delta t) - G_i(\boldsymbol{r}, t) = -\frac{\Delta t}{\tau_T}\left[G_i(\boldsymbol{r}, t) - G_i^{\mathrm{eq}}(\boldsymbol{r}, t)\right] \tag{5}$$

where ξ_i denotes the discrete particle velocity vectors, $\boldsymbol{r}$ is the position of particle at time t, and the time step Δt is considered to be one, and $F_i^{\mathrm{eq}}(\boldsymbol{r}, t)$ and $G_i^{\mathrm{eq}}(\boldsymbol{r}, t)$ are the particle equilibrium distribution function for flow and temperature fields, respectively. The relaxation times for the flow and temperature are denoted by τ_v and τ_T, respectively. In this work, the relaxation time ranges from 0.5 to 0.8. The buoyancy force term, f is used with the Boussinesq approximation.

The $F_i^{eq}(\boldsymbol{r},t)$ and $G_i^{eq}(\boldsymbol{r},t)$ local equilibrium distribution function terms use in eqs. (4) and ()5, respectively, can be written as:

$$F_i^{eq}(\boldsymbol{r},t) = \rho\omega_i\left[1+3\frac{(\vec{\xi}_i\vec{u})}{\xi^2}+\frac{9}{2}\frac{(\vec{\xi}_i\vec{u})^2}{\xi^4}-\frac{3}{2}\left(\frac{\vec{u}}{\xi}\right)^2\right] \tag{6}$$

$$G_i^{eq}(\boldsymbol{r},t) = \rho\omega_i\left[(1+3\frac{(\vec{\xi}_i\vec{u})}{\xi^2}\right] \tag{7}$$

where ρ is the fluid density and ω_i represents weighting factor for flow and temperature field. The thermal diffusivity, α, and kinematic viscosity, ν, are linked to the relaxation time in the following ways:

$$\nu = 0.5\xi^2(\tau_\nu - 0.5) \text{ and } \alpha = 0.5\xi^2(\tau_T - 0.5)$$

The discrete particle velocity vector and weighting factors for the D2Q9 lattice configuration are shown in tab. 1. Figure 1 depicts the lattice arrangement for the D2Q9 model.

With the help of the distribution function, we can easily enumerate macroscopic variables such as density, velocity and temperature as:

$$\rho = \sum_{i=0}^{8} F_i, \quad \boldsymbol{u} = \frac{1}{\rho}\sum_{i=0}^{8}\xi_i F_i, \text{ and } T = \sum_{i=0}^{8} G_i$$

Table 1. Weight functions and velocity vectors for D2Q9 lattice arrangements

i	ω_i	ξ_i
0	4/9	(0,0)
1	1/9	(1,0)
2		(0,1)
3		(–1,0)
4		(0,-1)
5	1/36	(1,1)
6		(–1,1)
7		(–1,–1)
8		(1,–1)

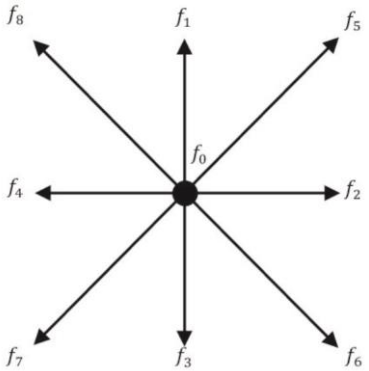

Figure 2. The sketch of D2Q9 model

Code validation

We initially investigate the streamline and temperature isotherms at Re = 10^3 and Gr = 10^6 to validate our developed code. According to the figure and tables, the present finding is consistent with Iwastu's *et al.* [10] results. Section *Results and discussions* includes details on the streamlines and temperature isotherms shown in the fig. 3. Figure 3 shows the comparison between stream lines and isotherms at Gr = 10^6 and Re = 10^3.

Tables 2 and 3 below compares the current result computed using LBM with the Iwastu *et al.* [10] results, at a fixed Grashof number.

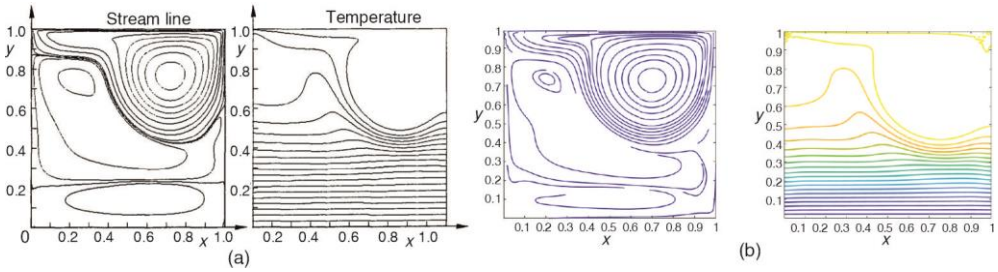

Figure 3. Comparison of stream lines and isotherms at Gr = 10^6 and Re = 10^3 between; (a) Iwastu's *et al.* [10] and (b) present results

Table 2. Comparison between the present results and Iwastu et al. [10] results at Gr = 10^2 and Re = 10^3

Re = 10^2	u_{min}	u_{max}	v_{min}	v_{max}
Iwastu *et al.* [10]	0.2037	1.0000	–0.2448	0.1698
Present	0.2007	1.0000	–0.2330	0.1655

Table 3. Comparison between the present results and Iwastu et al. [10] results at Gr = 10^2 and Re = 10^2

Re = 10^3	u_{min}	u_{max}	v_{min}	v_{max}
Iwastu *et al.* [10]	–0.3781	1.0000	–0.5178	0.3657
Present	–0.4007	1.0000	–0.5254	0.3822

Results and discussions

The ratio Gr/Re^2 is known as the Richardson number. It demonstrates the importance of natural convection driven by buoyancy effects over forced convection generated by the top sliding lid. It is worth mentioning that the results for a simple cavity are exactly similar to those of the research work of Iwastu *et al.* [10]. However, a square cavity with an internal heated or cold obstacle has not been studied yet. The horizontal velocity profile is plotted along $x = 0.5$ and the vertical velocity profile is plotted along $y = 0.5$ in all cases. If Ri $\ll$ 1, the mechanical action of the sliding lid overcomes the buoyancy effect. Figures 4-6 show the horizontal and vertical velocity profiles for Ri $\ll$ 1.

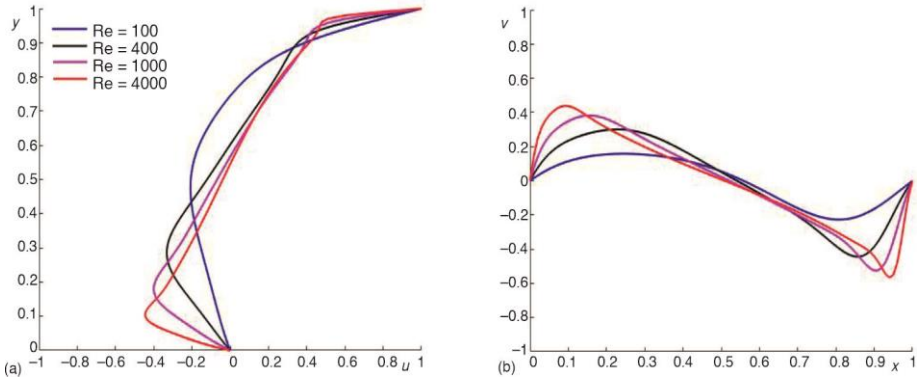

Figure 4. (a) horizontal and (b) vertical velocity profile at; Gr = 10^2 and Pr = 0.71

The qualitative characteristics of the flow are identical to those of the flow of non-stratified fluid in the classic lid-driven cavity. The development of boundary layer-like flow characteristics is seen at high Reynolds numbers. These properties have been thoroughly investigated in previous papers [8-10]. Since the bulk of fluid motion is circular, and buoyancy effects are negligible. That is why an obstacle in the centre of the cavity has no significant influence on the velocity of fluid in Cases 2 and 3. However, the velocity of the fluid decreases near the obstacle as compared to flow in a simple cavity without an obstacle.

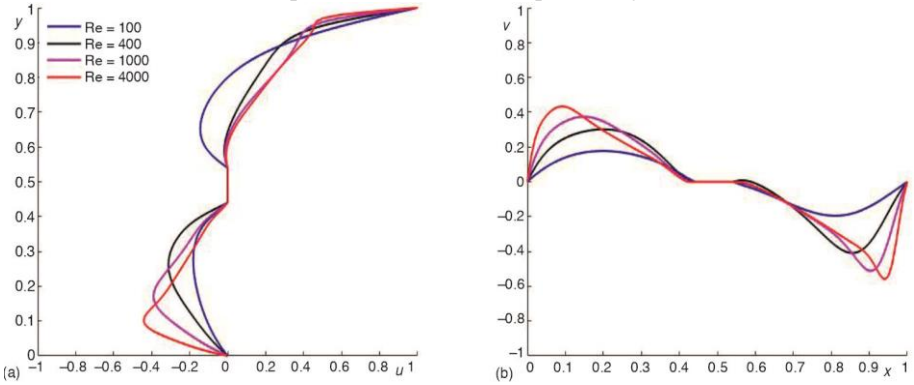

Figure 5. (a) horizontal and (b) vertical velocity profile at; Gr = 10^2 and Pr = 0.71 with internal square

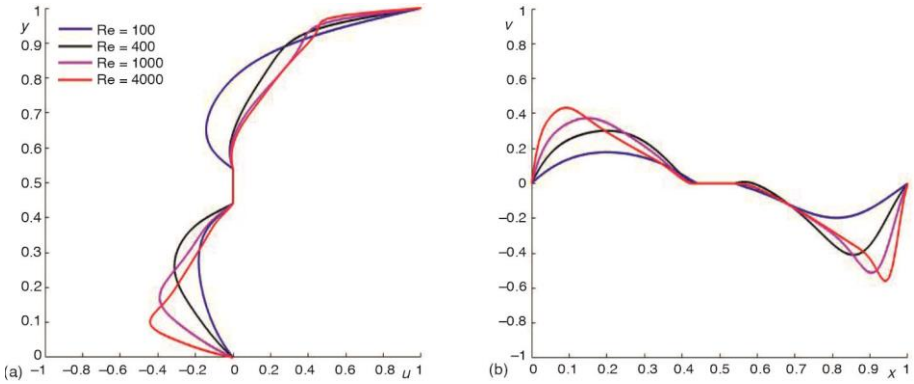

Figure 6. (a) horizontal and (b) vertical velocity profile at; Gr = 10^2 and Pr = 0.71 with heated square

Moreover, if Ri ≫ 1, the buoyancy effect takes priority over the mechanical effect of the sliding lid. Figures 7-9 shows velocity profile for Ri ≫ $O(1)$ and Ri ≪ 1. For Re = 100, 400, and 1000 we have Ri ≫ $O(1)$. As a result, the buoyancy effect takes priority. So, the fluid remains stagnant throughout the majority of the cavity. In Case 2, due to the cold obstacle, the temperature of the fluid around the obstacle decreases. As a result, the buoyancy effect becomes more dominant around the obstacles. That is why there is a substantial change in velocity near the obstacle. When we utilize a heated obstacle, the buoyancy effect reduces near the obstacle and fluid circulates in a much greater region than in Case 2. As a result, a change is seen in velocity near the obstacle. We have Ri ≪ 1 for Re = 3000, thus the results are the same as reported earlier.

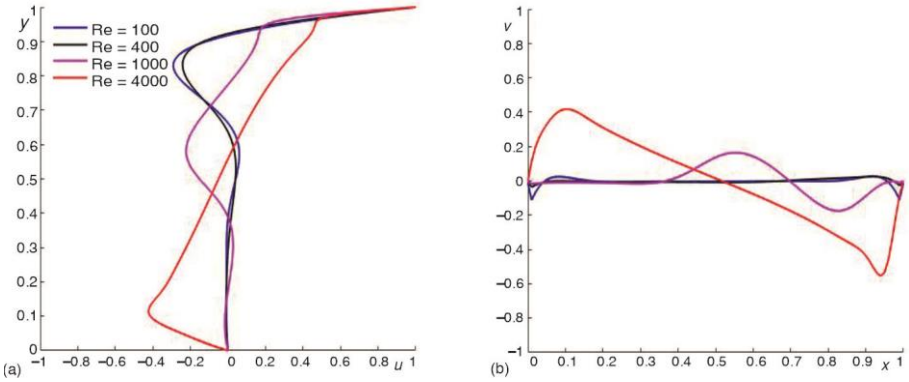

Figure 7. (a) horizontal and (b) vertical velocity profile at; Gr = 10^6 and Pr = 0.71

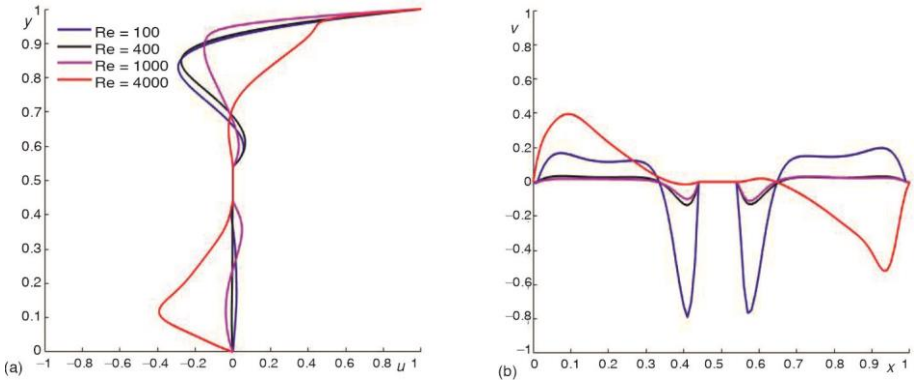

Figure 8. (a) horizontal and (b) vertical velocity profile at; Gr = 10^6 and Pr = 0.71 with internal square

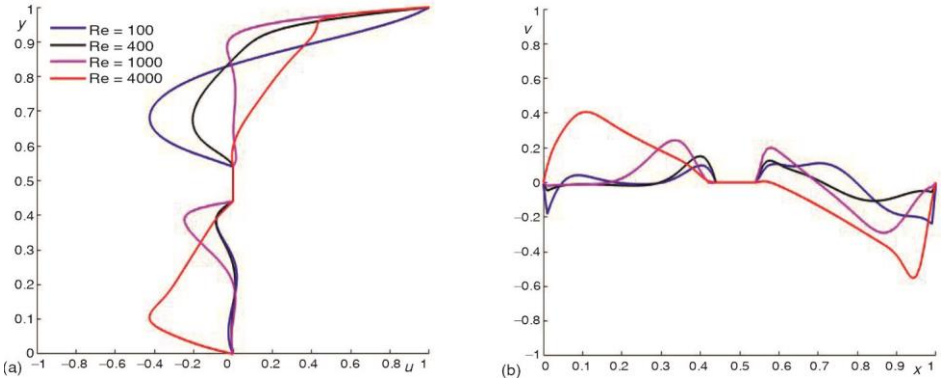

Figure 9. (a) horizontal and (b) vertical velocity profile at; Gr = 10^6 and Pr = 0.71 with heated square

The numerical results have been reorganised to show the change in fundamental row character as Grashof number grows at a fixed Reynolds number as shown in figs. 10-12. As the conditions Ri $\gg$ $O(1)$ and Ri $\ll$ 1 are firmly met, these results reveal the previously mentioned change in the major flow pattern.

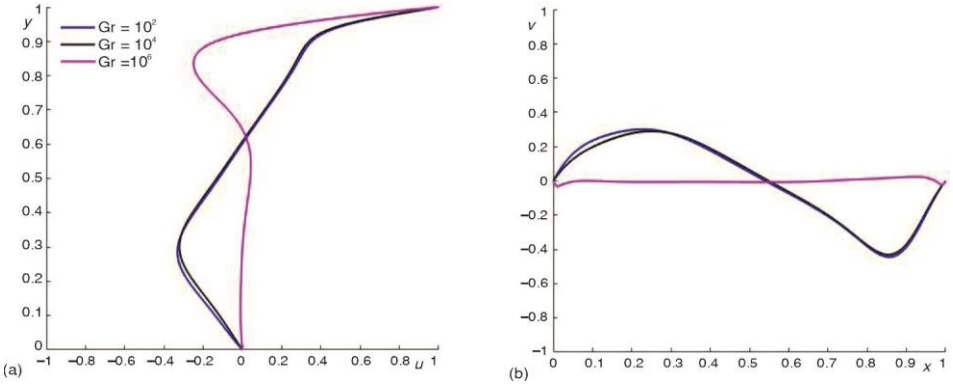

Figure 10. (a) horizontal and (b) vertical velocity profile at; Re = 400 and Pr = 0.71

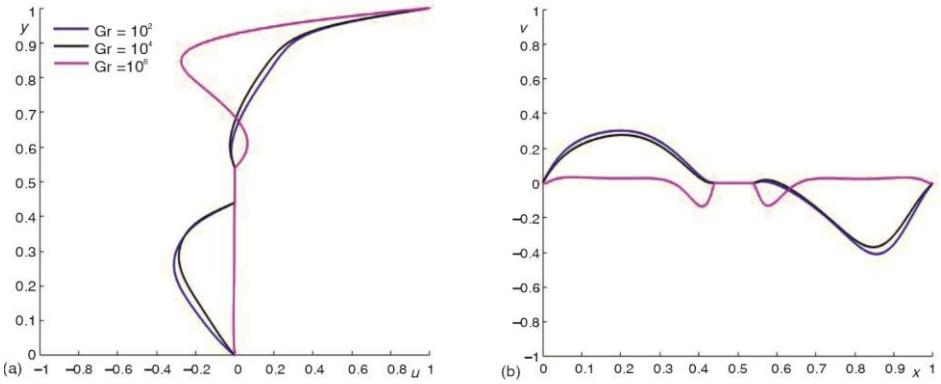

Figure 11. (a) horizontal and (b) vertical velocity profile at; Re = 400 and Pr = 0.71 with internal square

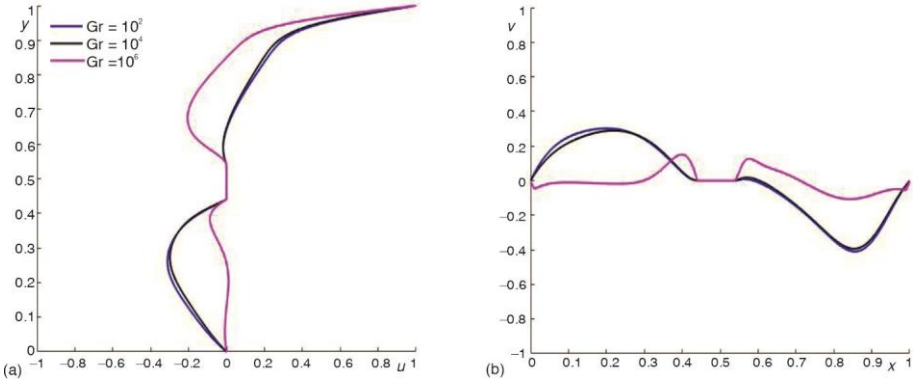

Figure 12. (a) horizontal and (b) vertical velocity profile at; Re = 400 and Pr = 0.71 with heated square

Figures 13 and 14 depicts the streamlines and temperature fields, respectively, for Ri ≪ 1 for each of the three cases. As a result, at comparable values of Reynolds number the overall flow characteristics of the figures are similar to those of a normal mechanically-driven cavity flow of a non-stratified fluid. Major circulation occupies the cavity's central

section, while smaller cells may be seen at the cavity's bottom corners. Streamlines are nearly identical in all cases. When an obstacle is added, the fluid-flow near the obstacle slows down slightly compared to a flow without an obstacle. Because buoyancy effects are insignificant, the temperature of obstacles has no impact on streamlines.

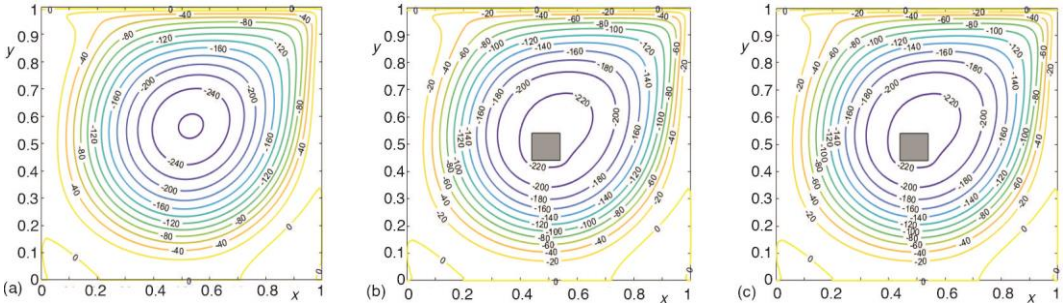

Figure 13. Variation of global flow with; (a) simple cavity, (b) internal cooled square, and (c) heated square at Re = 10^3 and Gr = 10^2

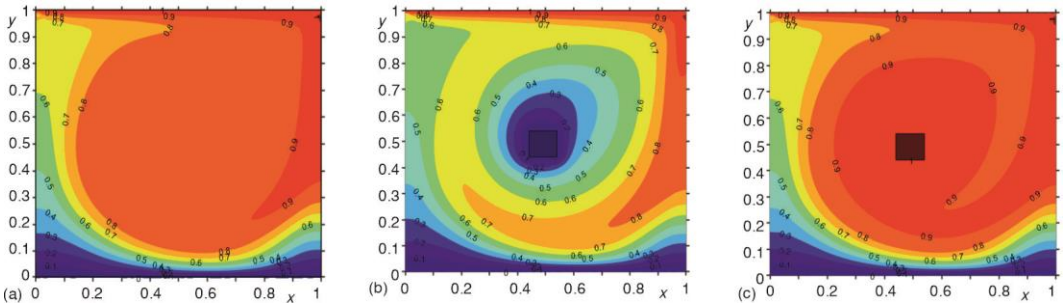

Figure 14. Variation of temperature of flow with; (a) simple cavity, (b) internal cooled square, and (c) heated square at Re = 10^3 and Gr = 10^2

As Ri $\ll 1$ indicates, natural convection has a negligible effect. Fluids are thoroughly mixed because of the strong effects of mechanically-driven circulations. As a result, much of the inner region has very small temperature variations in all three cases. Because of forced convection heat transfer from obstacle to surrounding region that's why, the temperature of the fluid near a cold obstacle is lower than in Case 1, and it rises as we go away from it in the circulation area. The temperature change in the presence of a heated obstacle is nearly identical to that in the absence of an obstacle, however, the temperature of the fluid surrounding the obstacle is slightly higher.

Figures 15 and 16 depicts the streamlines and temperature fields, respectively, for Ri $\sim O(1)$ for each of the three cases. In the case of Ri $\sim O(1)$ the buoyancy effects are likely to outweigh the impacts of the sliding wall. In comparison to the circulation region for Ri $\ll 1$, the internal circulation is confined to a narrow zone near to the sliding top lid because buoyancy factors now dominate over the sliding wall effect. The mechanically-driven top lid's impact only travels a short distance into the inner region. The steady stratification obviously prevents vertical movements. Much of the fluid in the middle and bottom interior areas remains stationary.

When a cooled obstacle is put into fluid, the buoyancy effects increase, so the fluid circulation is restricted to a narrower zone. Weak fluid circulation can also be visible in the

cavity's lower half. However, in all scenarios, the majority of the fluid remains stagnant in the bottom region of the cavity. When an obstacle is heated, the temperature surrounding it rises, reducing the buoyancy effect in the region and causing the fluid circulation zone to rise as it would in the absence of obstacles. The vertical temperature stratification in the stationary inner portions is nearly linear. This reflects the fact that heat transmission in the cavity's middle and bottom is mostly conductive. In a tiny zone near the top of the cavity, fluids are only fairly well mixed. In this zone, where mechanically generated convective activities are noticeable, the temperature is fairly stable.

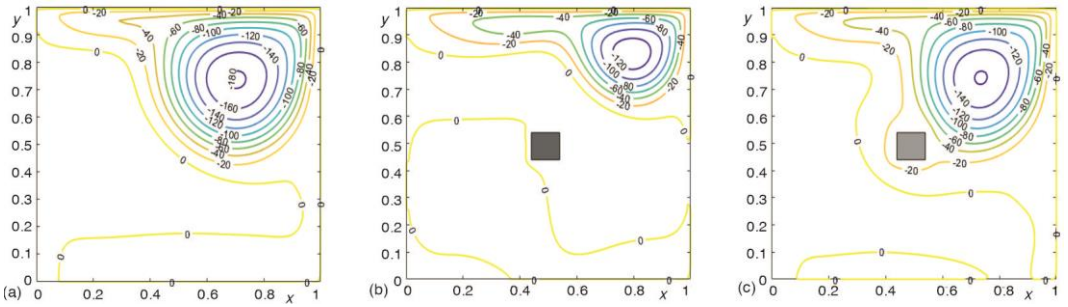

Figure 15. Variation of global flow with; (a) simple cavity, (b) internal cooled square, and (c) heated square at Re = 10^3 and Gr = 10^6

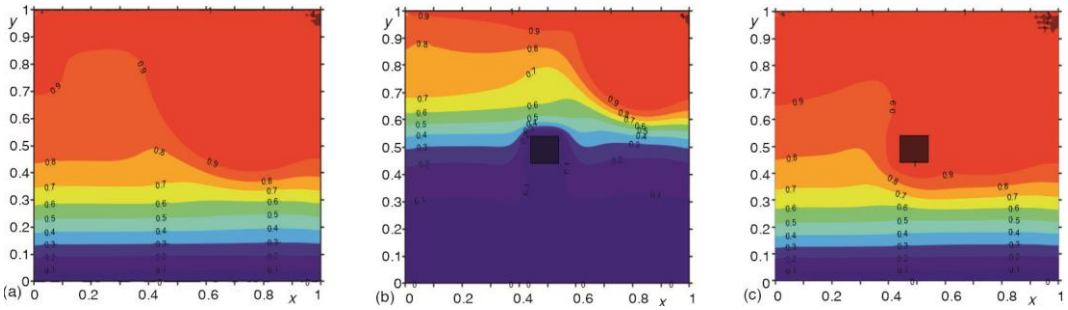

Figure 16. Variation of temperature of flow with; (a) simple cavity, (b) internal cooled square, and (c) heated square at Re = 10^3 and Gr = 10^6

The numerical results have been reorganised to show the change in temperature distribution as Grashof number grows at a fixed Reynolds number, as shown in fig. 17 . In all cases, the temperature profiles clearly fulfil the boundary conditions described in Section *Statement of the problem*. Because the conditions Ri $\gg$ $O(1)$ and Ri $\ll$ 1 are strictly met, these results show the previously specified change in the temperature profile. When Ri $\ll$ 1 we can see that forced convection contributes to the majority of heat transmission, whereas natural convection is negligible. When Ri = $O(1)$ both types of convection play a significant role. When Ri $\gg$ 1, forced convection becomes negligible.

More investigation was performed to see how the temperature of the fluid was affected by the Prandtl number. Figure 18 depicts the results. The temperature distribution in the interior tends to be vertically-linear for Pr $\ll$ 1. When Prandtl number is quite high, a strong circulation cell occupies the top half of the cavity interior, resulting in an area of well mixed fluids. As a result, the interior vertical temperature profile indicates a zone of rather constant temperature in the upper section of the cavity. In the case of Pr $\ll$ 1, the temperature of the obstacle has no noticeable influence as compared to high Prandtl number. However, in

the situation of high Prandtl number, the temperature of the obstacles affects the temperature of the fluid near the obstacles.

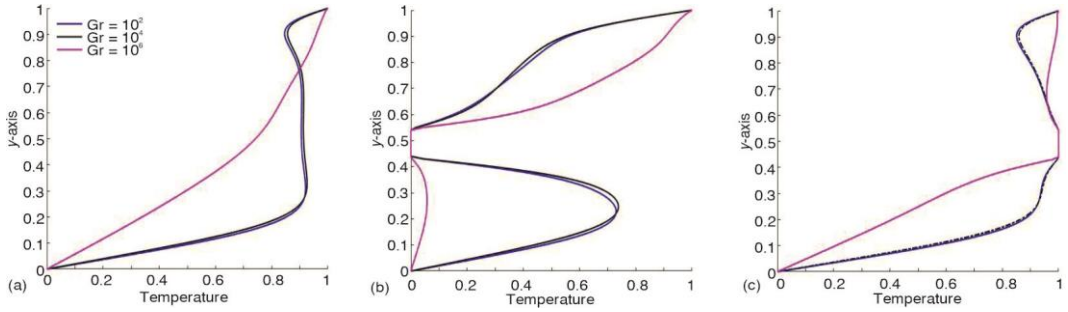

Figure 17. Vertical profile of temperature with; (a) simple cavity, (b) cooled obstacle, and (c) heated obstacle at Re = 10^3 and Pr = 0.71, x = 0.5

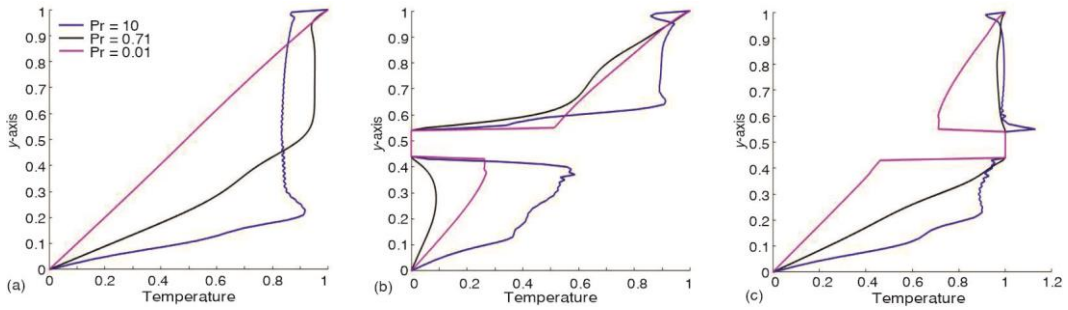

Figure 18. Vertical profile of temperature with; (a) simple cavity, (b) cooled obstacle, and (c) heated obstacle at Re = 10^3 and Gr = 10^6, x = 0.5

At a particular height, $\partial T/\partial y$ and $-\mathrm{PrRe}vT$ indicate the contributions of conductive and convective modes to total vertical heat transfer. Figures 19-21 shows the separated plots for both terms at various Grashof number with a fixed Re = 100. Convection is responsible for heat transport in the top and centre regions of the cavity when Ri $\leq O(1)$. On the other hand, when Ri $\gg$ 1 the graph clearly shows that the conductive method of heat transmission takes precedence over the convection mode. However, in the region surrounding heated and cold obstacles, both modes of heat transport play a significant role. This examination of the individual profiles of $\partial T/\partial y$ and $-\mathrm{PrRe}vT$ confirms the above-mentioned qualitative trends.

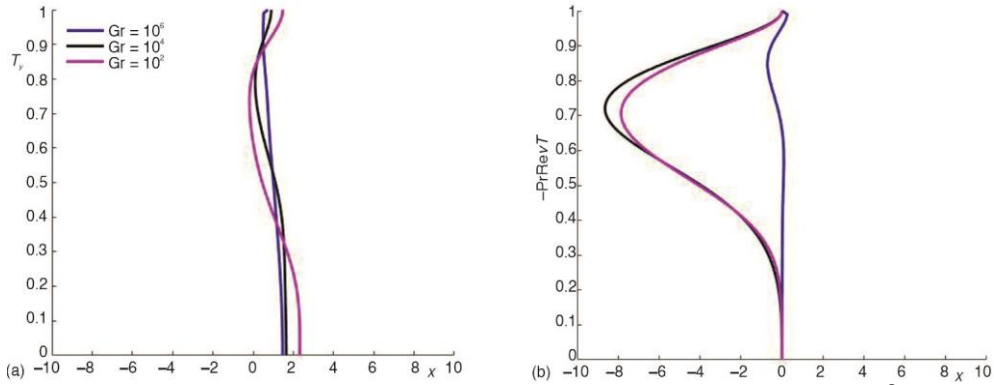

Figure 19. Vertical profile of; (a) T_y and (b) $-\mathrm{PrRe}vT$ along x = 0.5 at Re = 10^2

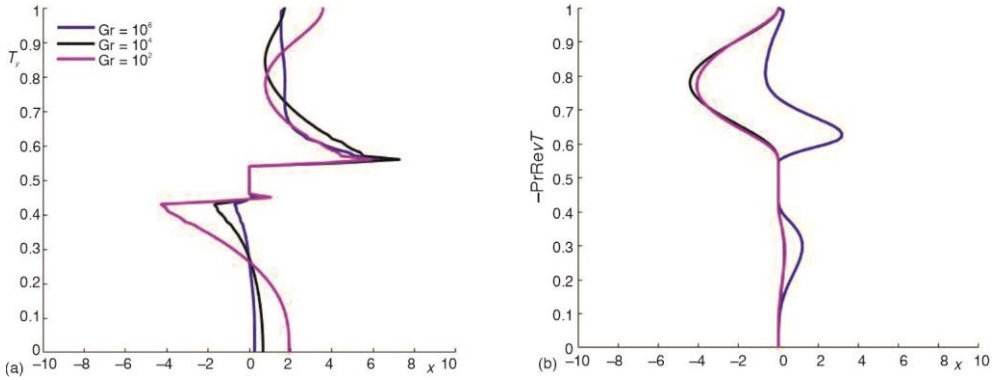

Figure 20. Vertical profile of;
(a) T_y and (b) –PrRevT along x = 0.5 at Re = 10^2 with cooled obstacle

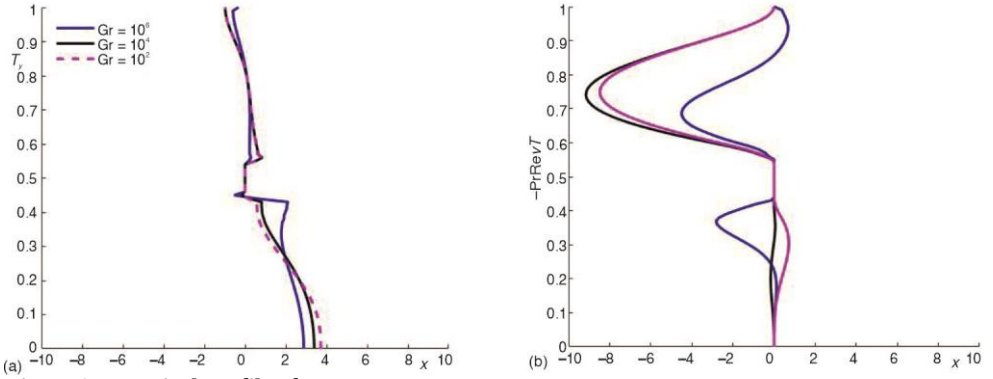

Figure 21. Vertical profile of;
(a) T_y and (b) –PrRevT along x = 0.5 at Re = 10^2 with heated obstacle

The practical design of heat transmission devices is heavily influenced by differences in local Nusselt numbers at the top and bottom walls. At Re = 400 and varying Grashof number, figures illustrate the Nusselt number profile at the top and bottom walls. Figure 22 depicts the Nusselt number for Ri ≪ 1, indicating when the convective mode of heat transport is dominating. The behaviour of the Nusselt number profiles at both boundary walls indicates the presence of significant fluid movements, which improves heat transmission throughout the cavity. Because the temperature differential near the top and bottom walls increases owing to the inner cold obstacle, the Nusselt number is larger on the top wall with cold obstacles as compared with heated or without obstacles. However, the findings for the heated obstacle are the same as in Case 1. As previously stated, the temperature differential is the same in both circumstances.

Figure 23 depicts the Nusselt number profile for Ri ≫ 1. Conduction dominates heat transfer in the interior, and fluid motions are generally subdued. As a result, Nusselt number at the bottom wall is getting closer to unity. Convective heat transport is fairly significant at the wall due to the presence of circulation near the top wall. As previously explained, when there is a cold obstacle, the temperature difference increases near the top wall. However, heat transfer at the bottom wall is totally conductive. The Nusselt number profile for the heated

obstacle is nearly identical to that of the bottom wall without an obstacle. However, with the exception of the top left corner, the temperature at the top wall is evenly distributed.

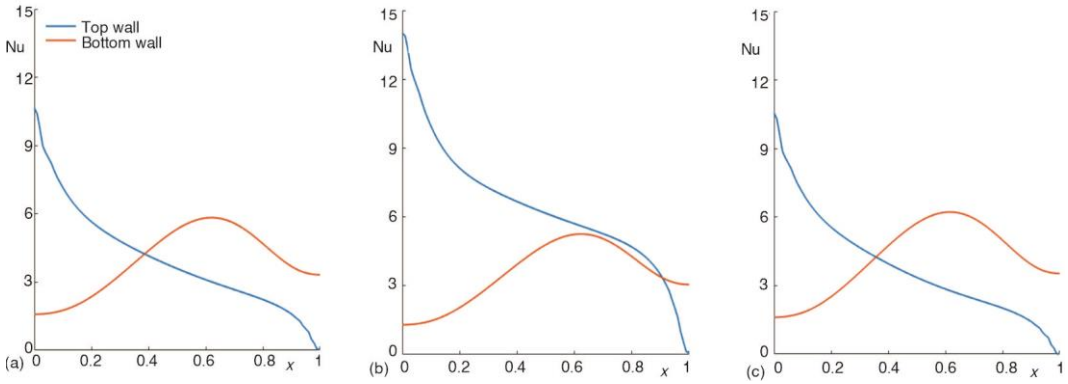

Figure 22. Local Nusselt number profile with; (a) simple cavity, (b) cooled obstacle, and (c) heated obstacle at Re = 400 and Gr = 10^2, x = 0.5

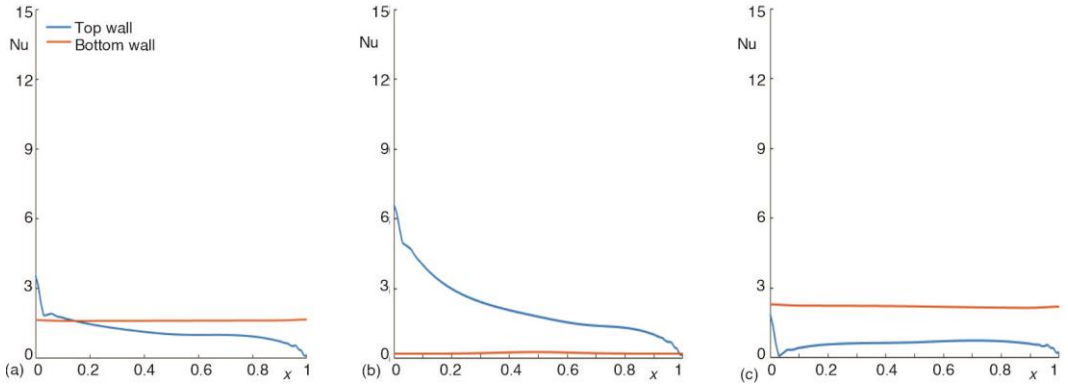

Figure 23. Local Nusselt number profile with; (a) simple cavity, (b) cooled obstacle, and (c) heated obstacle at Re = 400 and Gr = 10^6, x = 0.5

Conclusion

The numerical investigation of mixed convective flow and heat transfer in a square-shaped lid driven-cavity with an internal square-shaped obstacle located in the centre of the cavity was studied in detail using LBM.

When Ri $\ll$ 1 the buoyancy effect was overcome by the forced convection produced by the sliding lid. The majority of the cavity was covered by fluid circulation generated by the top wall, and temperature fluctuations were relatively linear in the circulation zone. The cold obstacle played an important role in reducing the effect of temperature transport in the central circulation zone. Furthermore, the obstacle in the centre of the cavity had produced no significant influence on velocity, both for a heated and a cold obstacle. Temperature distributions were almost identical in the case of a heated obstacle and without an obstacle. We conclude that convection was responsible for the bulk of heat transport, whereas conduction was minimal.

When Ri $\gg$ 1, the buoyancy effect was dominant. Fluid circulation was restricted to a small zone in the upper right half of the cavity. Much of the fluid at the bottom and in the

intermediate regions remained stagnant. In the bottom half, the isotherms were more horizontal, and a vertically-linear temperature distribution occurred. The results in the case of a heated obstruction were nearly identical to those in Case 1, with the exception of a tiny modification in the region around the obstacle. The circulation zone was confined to a smaller region when there was a cold obstacle as compared to a simple cavity or a cavity with a heated obstacle. Also, the temperature in the lower half of the cavity was almost zero. Conduction was responsible for the majority of heat transmission in this case, whereas convection was minimal.

The effect of Prandtl number on flow properties was investigated for Ri ~ $O(1)$. For Pr ≪ 1, the temperature distribution in the interior was almost vertically linear. A vigorous circulation cell filled the upper half of the cavity interior when Prandtl number was relatively high, resulting in a region of well-mixed fluids.

Additional examinations of the numerical results support the above-mentioned qualitative characteristics.

Nomenclature

A – aspect ratio, [–]
b – breadth of cavity
C – squared shaped body
$\mathbf{e}$ – unit vector in direction of buoyancy force
f – buoyancy force term
F^{eq} – equilibrium distribution function for fluid-flow
Gr – Grashof number, [–]
G^{eq} – equilibrium distribution function for temperature of fluid field
h – height of cavity
p – pressure field
Pr – Prandtl number, [–]
Re – Reynold number, [–]
Ra – Rayleigh number, [–]
$\mathbf{r}$ – buoyancy force term
T – temperature
T_h – temperature of top wall
T_o – temperature of bot-tom wall
Δt – time step
U_o – non dimensionalized lid velocity
$\mathbf{u}$ – non dimensionalized velocity
u,v – horizontal and vertical component of velocity
u_{min},u_{max} – minimum and maximum of horizontal component of velocity
v_{min},v_{max} – minimum and maximum of vertical component of velocity

Greek symbol

α – thermal diffusivity, [m^2s^{-1}]
ν – kinematic viscosity, [m^2s^{-1}]
τ_v – relaxation time for flow, [s^{-1}]
τ_T – relaxation time for temperature, [s^{-1}]
ρ – fluid density, [kgm^{-3}]
ξ – discrete particle velocity, [–]
ω – weighting factors, [–]

References

[1] Ghia, U. K. N. G., *et al.*, High-Re solutions for Incompressible Flow Using the Navier-Stokes Equations and a Multigrid Method, *Journal of Computational Physics, 48* (1982), 3, pp. 387-411
[2] Koseff, J. R., Street, R. L., Visualization Studies of a Shear Driven Three-Dimensional Recirculating Flow, *International Journal of Heat and Mass Transfer, 38* (1995), 18, pp. 3319-3328
[3] Koseff, J. R., Street, R. L., On End Wall Effects in a Lid-Driven Cavity Flow, *Journal of Fluids Engineering, 106* (1984), 4, pp. 385-389
[4] Koseff, J. R., and Street, R.L., 1984. The lid-driven cavity flow: a synthesis of qualitative and quantitative observations, *Journal of Fluids Engineering, 106* (1984), pp.390-398.
[5] Schreiber, R. Keller, H. B., Driven Cavity Flows by Efficient Numerical Techniques, *Journal of Computational Physics, 49* (1983), 2, pp. 310-333
[6] Freitas, C. J., *et al.*, Numerical Simulation of Three-Dimensional Flow in a Cavity, *International Journal for Numerical Methods in Fluids, 5* (1985), 6, pp. 561-575
[7] Perng, C. Y., Street, R. L., Three-Dimensional Unsteady Flow Simulations: Alternative Strategies for a Volume-Averaged Calculation, *International Journal for Numerical Methods in Fluids, 9* (1989), 3, pp. 341-362

[8] Iwatsu, R., *et al.*, Numerical Simulation of Three-Dimensional Flow Structure in a Driven Cavity, *Fluid Dynamics Research, 5* (1989), 3, 173
[9] Iwatsu, R., *et al.*, Analyses of Three-Dimensional Flow Calculations in a Driven Cavity, *Fluid Dynamics Research, 6* (1990), 2, 91
[10] Iwatsu, R., *et al.*, Mixed Convection in a Driven Cavity with a Stable Vertical Temperature Gradient, *International Journal of Heat and Mass Transfer, 36* (1993), 6, pp. 1601-1608
[11] Mohamad, A. A., Viskanta, R., Combined Surface Shear and Buoyancy-Driven Convection in a Shallow Cavity, *Fundamentals of Natural Convection, 140* (1990), pp.1-7
[12] Karimipour, A., *et al.*, Mixed Convection of Copper-Water Nanofluid in a Shallow Inclined Lid Driven Cavity Using the Lattice Boltzmann Method, *Physica A: Statistical Mechanics and Its Applications, 402* (2014), May, pp. 150-168
[13] Guo, Y., *et al.*, Simulation of Mixed Convection in Slender Rectangular Cavity with Lattice Boltzmann Method, *International Journal of Numerical Methods for Heat and Fluid-Flow, 20* (2008), 1, pp. 130-148
[14] Bettaibi, S., *et al.*, Lattice Boltzmann Simulation of Mixed Convection Heat Transfer in a Driven Cavity with Non-Uniform Heating of the Bottom Wall, *Communications in Theoretical Physics, 63* (2015), 1, 91
[15] Abu-Nada, E., Chamkha, A. J., Mixed Convection Flow of a Nanofluid in a Lid-Driven Cavity with a Wavy Wall, *International Communications in Heat and Mass Transfer, 57* (2014), Oct., pp. 36-47
[16] Oztop, H. F., *et al.*, MHD Mixed Convection in a Lid-Driven Cavity with Corner Heater, *International Journal of Heat and Mass Transfer, 54* (2011), 15-16, pp. 3494-3504
[17] Ouhroum, M., *et al.*, Numerical Study of Mixed Convection in Square Cavity Using Lattice Boltzmann Method: Cavity with Many Dispositions of Obstacles, *AIP Conference Proceedings 2345* (2021), 1, 020012
[18] Walther, E., Contribution of Lattice Boltzman Methode to the Study of the Building Envelope (in Franch), Ph. D. thesis, Universite Paris-Saclay, Paris, France, 2016
[19] Peng, Y., *et al.*, Simplified Thermal Lattice Boltzmann Model for Incompressible Thermal Flows, *Physical Review E, 68* (2003), 2, 026701
[20] Chen, H., Teixeira, C., H-Theorem and Origins of Instability in Thermal Lattice Boltzmann Models, *Computer Physics Communications, 129* (2000), 1-3, pp. 21-31
[21] Bhatnagar, P. L., *Et Al.*, A Model For Collision Processes In Gases. I. Small Amplitude processes in Charged and Neutral Onecomponent Systems, *Physical review, 94* (1954), 3, 511
[22] Zou, Q., He, X., On Pressure and Velocity Boundary Conditions for the Lattice Boltzmann BGK Model, *Physics of Fluids, 9* (1997), 6, pp. 1591-1598

Paper submitted: February 16, 2022
Paper revised: June 15, 2022
Paper accepted: June 17, 2022